ADVANCED MATERIALS
www.advmat.de

A 2D Titanium Carbide MXene Flexible Electrode for High-Efficiency Light-Emitting Diodes

Soyeong Ahn, Tae-Hee Han, Kathleen Maleski, Jinouk Song, Young-Hoon Kim, Min-Ho Park, Huanyu Zhou, Seunghyup Yoo, Yury Gogotsi, and Tae-Woo Lee**

Although several transparent conducting materials such as carbon nanotubes, graphene, and conducting polymers have been intensively explored as flexible electrodes in optoelectronic devices, their insufficient electrical conductivity, low work function, and complicated electrode fabrication processes have limited their practical use. Herein, a 2D titanium carbide (Ti_3C_2) MXene film with transparent conducting electrode (TCE) properties, including high electrical conductivity (≈11 670 S cm^{-1}) and high work function (≈5.1 eV), which are achieved by combining a simple solution processing with modulation of surface composition, is described. A chemical neutralization strategy of a conducting-polymer hole-injection layer is used to prevent detrimental surface oxidation and resulting degradation of the electrode film. Use of the MXene electrode in an organic light-emitting diode leads to a current efficiency of ≈102.0 cd A^{-1} and an external quantum efficiency of ≈28.5% ph/el, which agree well with the theoretical maximum values from optical simulations. The results demonstrate the strong potential of MXene as a solution-processable electrode in optoelectronic devices and provide a guideline for use of MXenes as TCEs in low-cost flexible optoelectronic devices.

Dr. S. Ahn, Prof. T.-H. Han, Dr. Y.-H. Kim, Dr. M.-H. Park, H. Zhou, Prof. T.-W. Lee
Department of Materials Science and Engineering
Institute of Engineering Research
Research Institute of Advanced Materials
BK21 PLUS SNU Materials Division for Educating Creative Global Leaders
Seoul National University
1 Gwanak-ro, Gwanak-gu, Seoul 08826, Republic of Korea
E-mail: twlees@snu.ac.kr

Prof. T.-H. Han
Division of Materials Science and Engineering
Hanyang University
222 Wangsimni-ro, Seongdong-gu, Seoul 04763, Republic of Korea

Dr. K. Maleski, Prof. Y. Gogotsi
A.J. Drexel Nanomaterials Institute and Department of Materials Science and Engineering
Drexel University
3141 Chestnut Street, Philadelphia, PA 19104, USA
E-mail: gogotsi@drexel.edu

J. Song, Prof. S. Yoo
School of Electrical Engineering
Korea Advanced Institute of Science and Technology (KAIST)
291 Daehak-ro, Yuseong-gu, Daejeon 34141, Republic of Korea

The ORCID identification number(s) for the author(s) of this article can be found under https://doi.org/10.1002/adma.202000919.

DOI: 10.1002/adma.202000919

Indium tin oxide (ITO) has been being widely used as a transparent conducting electrode (TCE) for optoelectronic devices, but it has a number of disadvantages such as brittleness, high and further increasing cost, and diffusion of metal species into devices.[1–6] Several other flexible conducting materials including carbon nanotubes, graphene and conducting polymers have been considered as an alternative solution, providing flexibility to the TCE and their usages were intensively explored for flexible optoelectronics.[6–20] Even though there has been substantial progress in flexible optoelectronic applications, still a number of technical issues remain. To achieve high quality graphene, a high-temperature chemical vapor deposition (CVD) growth at ≈1000 °C, and additional charge transfer doping are usually required to improve the electrical conductivity σ of intrinsic graphene sheets.[6,21–23] The graphene doped with volatile chemicals has electrical instability issues, complicating fabrication of devices.[23–26] Conducting polymers (e.g., poly(3,4-ethylenedioxythiophene) polystyrene sulfonate (PEDOT:PSS)) have been limited by the relatively low electrical conductivity (<1000 S cm^{-1}).[27–29] Furthermore, the work function (WF) of both conducting materials are usually less than 4.8 eV, which also acts as a critical limiting factor for organics, quantum dots, and perovskite light-emitting diodes (LEDs) due to a large energy barrier formation for hole injection.

MXenes are 2D transition-metal carbides, nitrides, or carbonitrides that have the formula $M_{n+1}X_n$, where M is an early transition metal (e.g., Ti, V, Nb, and Mo), and X is C, N, or both.[30,31] They have metallic conductivity ($5000 \leq \sigma \leq 10\,000$ S cm^{-1}), which is a result of metal-like high free-electron density and a sheet-like structure of individual nanosheets.[32] MXenes have surface hydrophilicity which provides an excellent platform for solution-processing approaches.[30–34] MXenes are fabricated using a wet chemical synthesis procedure, which leaves surfaces that are terminated by functional groups such as –OH, –O, –Cl, and –F, which make the MXenes dispersible in polar solvents.[35] Grafting approaches can be used to enable dispersion in nonpolar solvents.[36] Due to the 2D structure and high electrical conductivity along with the simple fabrication, MXenes have been explored as electrodes and current collectors of metal ion batteries, sensors, gas and electrochemical storage

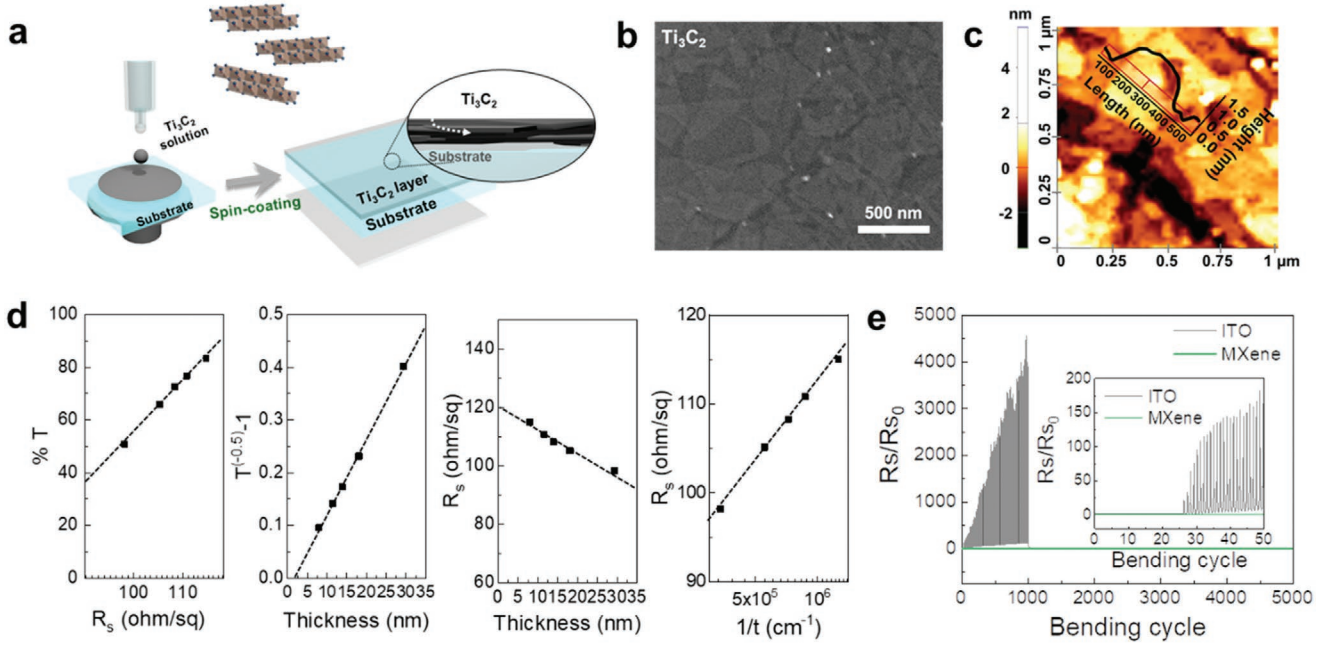

Figure 1. a) Schematic illustration of MXene film formation using Ti_3C_2 MXene solution by spin-coating on ozone-treated substrate. b) SEM and c) AFM images of prepared Ti_3C_2 film. d) Characterization of optoelectronic properties. From left to right: transmittance T (%) versus sheet resistance R_S (Ω sq^{-1}); slope of ($T^{0.5}-1$) versus thickness yields optical conductivity (S cm^{-1}); slope of R_S versus thickness (cm) or inverse thickness (cm^{-1}) yields DC conductivity (S cm^{-1}). e) R_S normalized to initial value R_{S0} of ITO and MXene after bending up to 5000 times.

media, energy devices, and catalysts.[37–46] Metallic conductivity and hydrophilic surface make MXenes good candidates for use as solution-processed TCEs for flexible optoelectronic devices. However, MXene have not been properly used for supporting an LED because the MXene films can be severely damaged when they are coated with an acidic-water-based hole-injection layer (HIL).[32,33,47] The surface functional groups substantially affect the electrical and electronic properties of MXenes.[48] Oxidation of MXene film significantly degrades its σ and decreases its WF. In a TCE, these changes could alter the charge balance in LEDs and significantly decrease their luminous efficiencies, and this result impedes use of MXene TCEs in optoelectronic devices.

In this work, we exploited single-layered Ti_3C_2 MXene as a solution-processed flexible TCE, and used a one-step spin-coating and low-temperature vacuum-annealing protocol to obtain MXene electrode films that have substantially high σ (up to 11 668 S cm^{-1} and 108 Ω sq^{-1}), high WF (≈5.1 eV), and good optical transmittance T (up to 85%). To overcome the major degradation of the MXene film during device fabrication, we used low-temperature vacuum annealing to modulate the surface of the MXene film, thus protecting the high σ and high WF. We also used a chemically neutralized alcohol-based HIL to protect the material from interface oxidation. The effectiveness of our strategies to engineer the surface and interface was demonstrated by analysis of the chemical compositions of MXene films, and by the nearly ideal charge injection (hole-injection efficiency ≈1) from the modified MXene film to the overlying hole transporting layer (HTL). Phosphorescent organic LEDs with a modified MXene anode showed high efficiency (current efficiency ≈101.9 cd A^{-1}; external quantum efficiency ≈28.5% ph/el), and show the great potential of MXenes as solution-processed flexible TCE for LEDs.

Ti_3C_2 MXene film was prepared by spin-casting of the Ti_3C_2 solution for flexible transparent electrode application (**Figure 1**a). The individual MXene nanosheets in the film overlapped (Figure 1b); each MXene nanosheet was ≈1 nm-thick (Figure 1c), which closely matches the theoretical value of monolayer Ti_3C_2.[34,49] T of the MXene film could be widely controlled from 50 to 85% at 550 nm (Figure S1, Supporting information), and the sheet resistance (R_S) of the film could be tuned from 98 to 115 Ω sq^{-1} (Figure 1d) by adjusting its thickness (t) from 29 to 79 nm. The maximum $\sigma = 1/(R_S \cdot t)$ of the MXene film was 10 957 S cm^{-1}, which is notably high among flexible conducting films.[15,50–52]

In bending tests (bending radius 3 and 1 mm (Figure S2, Supporting information)), the MXene electrode fabricated on a 130 µm-thick poly(ethylene terephthalate) (PET) substrate showed good flexibility and cycling stability, whereas the conventional ITO electrode on PET substrate cracked after a few cycles of bending. As a result of the poor mechanical properties of ITO, its electrical properties also decreased as the number of bending cycles increased. In R_S measurements, the MXene electrode on PET did not show any change after 5000 bending cycles, whereas the ITO on PET showed a sharp increase in R_S after 1000 bending cycles (Figure 1e). The MXene film composed of overlapped nanosheets network can effectively retain the electrical coupling between individual MXene sheets under high and cyclic mechanical stress (Figure S2, Supporting information).

The surface WFs of MXene and ITO electrode films were compared by measuring their spatial surface potentials with Kelvin probe. As-prepared MXene film had a higher WF (≈5.0 eV) than the ITO electrode (≈4.8 eV) (**Figure 2**a). The MXene nanosheets are terminated with functional groups such as –OH, –O, –Cl, and –F after the solution preparation process

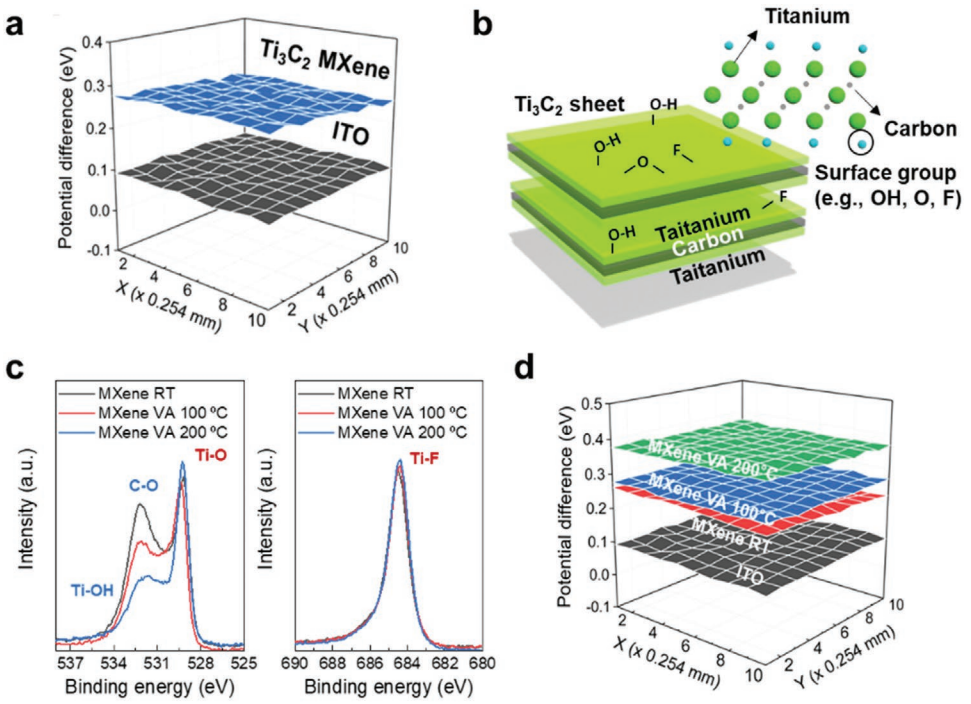

Figure 2. a) Contact potential difference (CPD) of ITO and Ti_3C_2 MXene electrodes measured by Kelvin probe. b) Schematic illustration of MXene sheets and their surface functional groups (–OH, –O, and –F). c) XPS O 1s, F 1s spectra and d) CPD of MXene films with low-temperature vacuum annealing at 100, and 200 °C, or dried at RT (≈23 °C) without vacuum annealing, with ITO as a comparison.

(Figure 2b). Functional groups on MXene flakes can change the resulting WF by changing the surface dipoles of MXene (i.e., by shifting the Fermi energy level of the metallic semiconductor).[53,54] Density functional theory (DFT) predicted that the WF of Ti_3C_2 can be in a wide range from 1.6 eV with hydroxyl (–OH) surface termination to 6.25 eV with oxygen (–O) surface termination).[53]

The anode WF strongly influences the charge carrier injection as a result of formation of an energy barrier with the highest occupied molecular orbital (HOMO) energy levels of the overlying organic layer (HIL), so a high WF is desirable for efficient charge injection, which can translate directly to high efficiency of LEDs.[2,6,15,55] The MXene WF of 5.0 eV is higher than those of other flexible electrodes (e.g., pristine graphene: ≈4.4 eV; high-σ PEDOT:PSS: ≈4.8 eV), but the usual organic/polymeric HIL has HOMO energy >5.2 eV, so a small energy barrier still exists.

To further increase the WF of MXene, we used vacuum annealing to remove –OH surface functional groups and thereby increase the ratio of –O to –OH surface terminations on the MXene film. To verify the ratio of the functional groups, X-ray photoelectron spectroscopy (XPS) of MXene films were analyzed according to annealing processes (dried at room temperature, vacuum-annealed at 100 °C for 1 h or 200 °C for 2 h) (Figure 2c). This process noticeably decreased the –OH terminated Ti (534 eV in O 1s spectra) and the C–O contamination (532.2 eV), so the ratio of –O terminated Ti (529.3 eV) and –F terminated Ti (684 eV in F 1s spectra) on the film surface increased slightly as annealing temperature and time were increased. As a result, the WF of the MXene film after vacuum annealing at 200 °C increased to ≈5.1 eV (Figure 2d; Figure S3, Supporting information). The higher vacuum annealing temperature (250 °C) begins to decrease WF of MXene film possibly due to high-temperature-induced loss of fluorine termination (Figure S4, Supporting information). The air-photoemission measurement provided further evidence that the WF increased in the MXene film after vacuum annealing (Figure S5, Supporting information). Also, the low-temperature vacuum annealing and concomitantly altered surface chemical composition increased the σ of the MXene film to 11 668 S cm^{-1} (R_S = 108 Ω sq^{-1}) after annealing in vacuum at 200 °C for 2 h.

An MXene electrode should not react with the overlying solution-processed HIL. However, humid and acidic environments oxidize Ti_3C_2 MXene.[56,57] The influence of water and acid permeation on the chemical compositions of Ti_3C_2 MXene film was investigated by XPS analysis. Composition changes of Ti_3C_2 were observed after water and acid exposure on the MXene film (Figure S6, Supporting information). The TiO_2 peak centered at 458.5 eV in the XPS Ti 2p spectrum strengthened after exposure to deionized water or hydrochloric acid; these changes imply that Ti_3C_2 on the surface of the film is oxidized. This result also indicates that the acidity of HIL also accelerates the oxidization of Ti_3C_2 MXene electrode films, so σ of the electrode decreases (Figures S3 and S4, Supporting information). Also, the application of the conventional polymeric HIL, PEDOT:PSS to MXene-coated substrate caused Ti_3C_2 sheets to delaminate from the substrate (**Figure 3**a). This result could be also attributed to permeation of water into the Ti_3C_2 layers due to hydrophilic –OH and –O surface terminations of the Ti_3C_2 sheets, and to the acidic nature of PEDOT:PSS that could oxidize the MXene

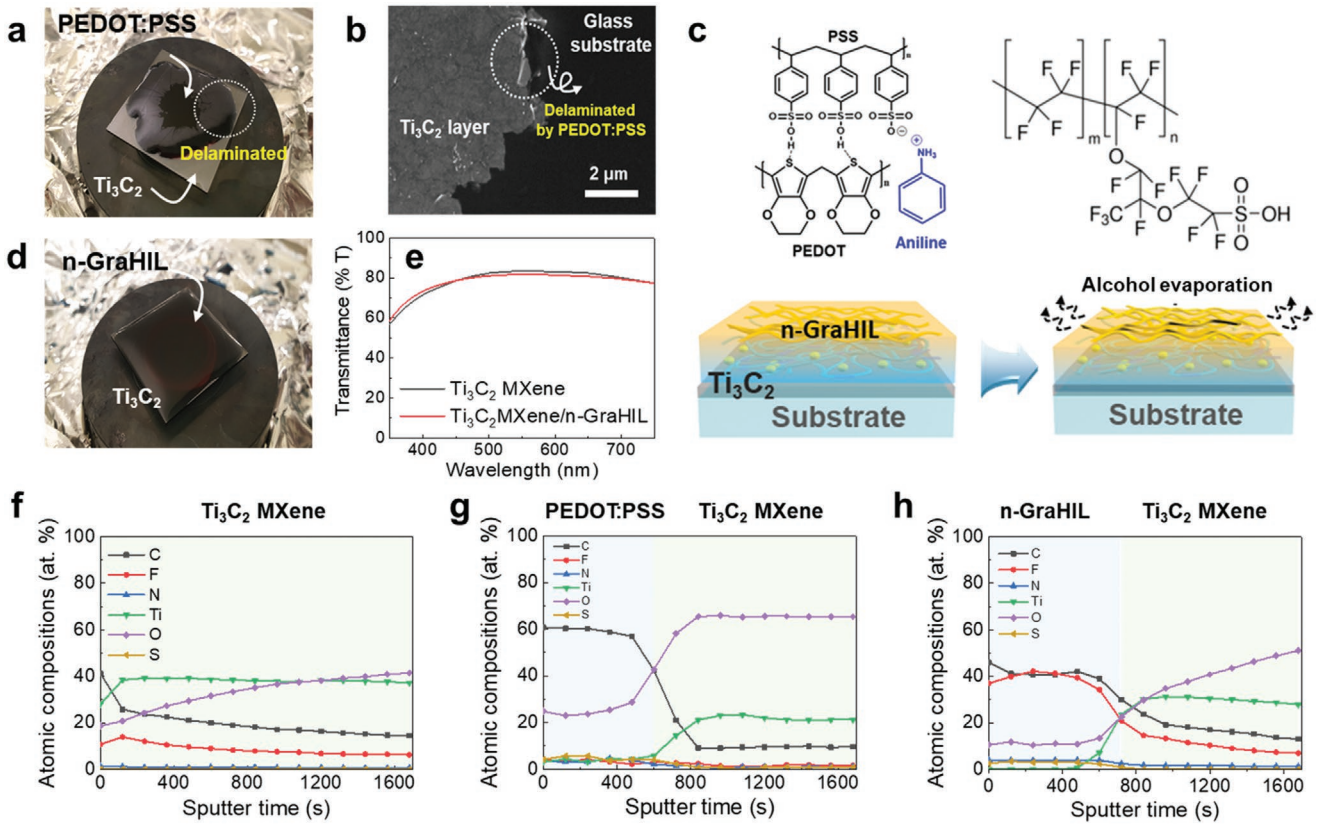

Figure 3. a) Delamination of Ti_3C_2 MXene during spin-coating of PEDOT:PSS and b) SEM images of delaminated MXene film. c) Chemical structures of constituents (PEDOT:PSS, aniline and perfluorinated polymer) of n-GraHIL, and schematic of n-GraHIL formation on Ti_3C_2 MXene film. d) MXene uniformly covered by n-GraHIL solution without delamination, and e) transmittance of MXene films without and with n-GraHIL. f–h) XPS depth profiles of Ti_3C_2 MXene (f), MXene/PEDOT:PSS (g), and MXene/n-GraHIL (h).

film. XPS depth profiles of bare Ti_3C_2 and PEDOT:PSS-coated Ti_3C_2 revealed that water-dispersed PEDOT:PSS diffused throughout the Ti_3C_2 film (Figure 3f,g). Judging from the atomic concentrations of C and S, the depth profile was divided into HIL and Ti_3C_2 MXene regions (Figure 3f–h). The atomic concentration of oxygen in the MXene film (where the concentration of C is reduced) increased significantly compared to that of bare Ti_3C_2 after spin-coating of PEDOT:PSS on MXene film (Figure 3g).

To avoid the water/acid permeation and delamination of the MXene electrodes, a chemically neutralized polymeric HIL (n-GraHIL) was introduced in LED applications. The conventional PEDOT:PSS was neutralized by incorporating Lewis-basic aniline molecules into the PEDOT:PSS solution to chemically coordinate acidic polystyrene sulfonic acid (PSS) moieties in the PEDOT:PSS (Figure 3c), so the pH of our n-GraHIL was tuned to be near 7. The n-GraHIL also contains a perfluorinated polymer that has low surface energy and high ionization potential, thereby additionally developing a gradient WF inside the HIL (surface WF: ≈5.95 eV) and yielding efficient hole injection into the emitting layer (EML).[2,6,55,58] The water content in the n-GraHIL solution was reduced by replacing water with alcohol as a solvent for the polymer blends so that water permeation into the electrode film could be reduced during the solution process compared to the process that used water-based solution.

The pH-neutral and alcohol-based HIL was used to avoid oxidation, and did not cause delamination of Ti_3C_2 layers during spin-coating (Figure 3d). The n-GraHIL film formed uniformly on the Ti_3C_2 electrode film and did not show significant effect on its *T* (Figure 3e). These results can be attributed to the neutral environment and to the faster evaporation of alcohol-based solvent than water during HIL formation on the MXene film (Figure 3c). The fast solvent evaporation of n-GraHIL did not allow time for diffusion into Ti_3C_2 sheets, or for surface oxidation of the electrode film. The atomic concentration of oxygen and the ratio of O/Ti did not change much from the XPS depth profile of bare Ti_3C_2 (Figure 3h; Figure S8, Supporting information).

To evaluate the hole-injection capability from the MXene anode/n-GraHIL stack, we fabricated hole-only devices (HODs) (**Figure 4**a). At low voltage, the voltage-current density curves of the HODs with Ti_3C_2 MXene anode showed higher hole-current density at a given applied bias than did the HODs that used a conventional ITO anode; this result can be attributed to MXene anode's higher WF (≈5.1 eV) than that of ITO (≈4.8 eV) (Figure 4b). The hole-injection efficiency of MXene/n-GraHIL was calculated by comparison with a theoretical space charge-limited current (SCLC) model and Poole–Frenkel equations (Figure 4c and Supporting Information). The MXene/n-GraHIL showed hole-injection efficiency ≈1, which means that Ohmic-like hole injection is achievable

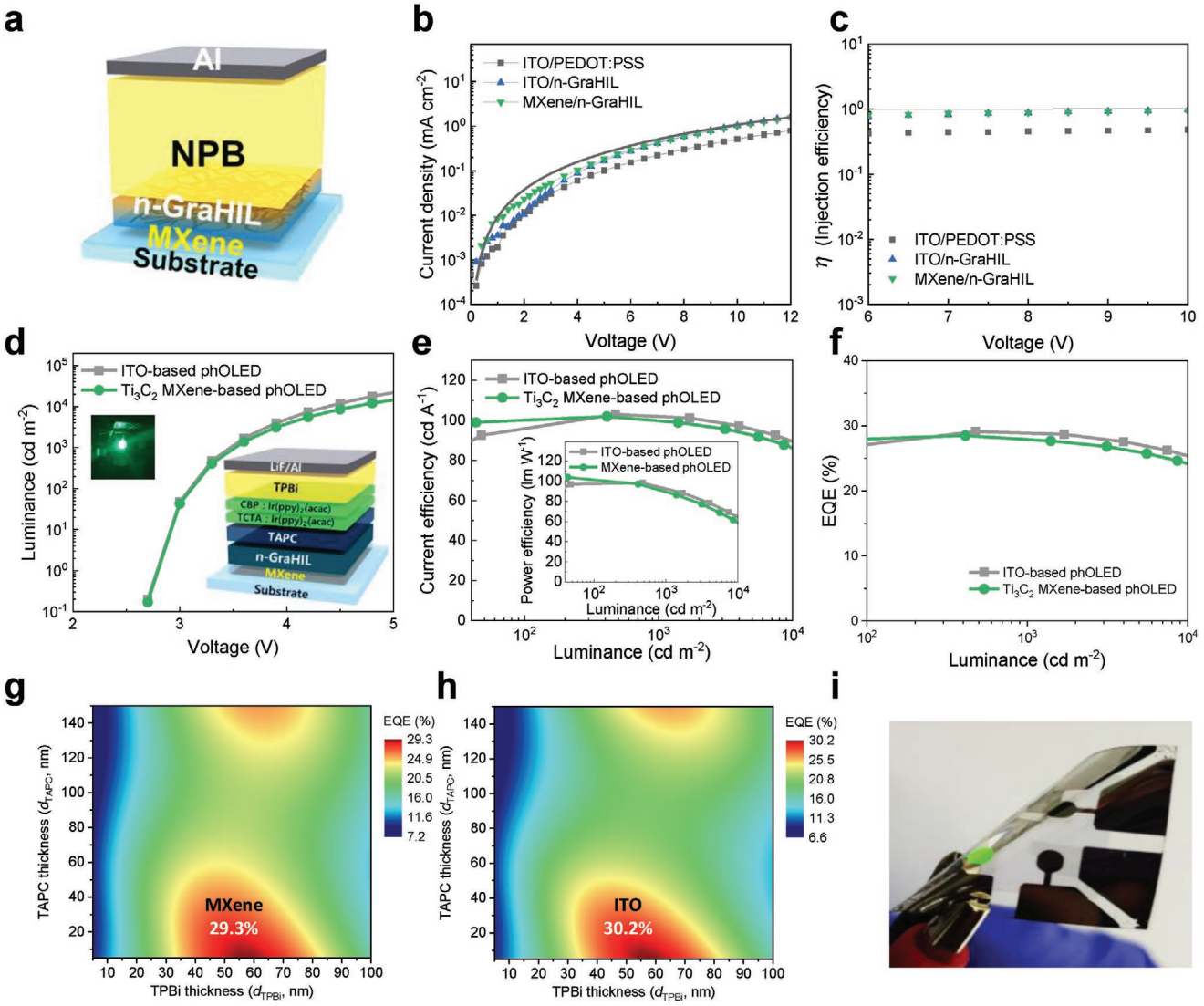

Figure 4. a) Schematic illustration of the hole-only device design, b) current density versus voltage characteristics, and c) calculated hole-injection efficiency η of hole-only device with ITO/PEDOT:PSS, ITO/n-GraHIL and MXene/n-GraHIL. d) Luminance versus voltage characteristics of LEDs that have ITO or MXene electrode (inset: optical image of MXene-based green organic LED (left), and schematic of green phosphorescent organic LED device structure (right)). e) Current efficiency versus luminance characteristics (inset: power efficiency versus luminance characteristics), and f) EQE versus luminance characteristics of LEDs using ITO and MXene as electrodes. g,h) Calculated maximum EQE of organic LEDs with MXene (g) and ITO (h) electrode as a function of functional layer thickness, and i) optical image of flexible organic LEDs based on MXene electrodes.

using a MXene anode with engineered surface and interface chemical composition.

We also fabricated green phosphorescent organic LEDs that had solution-processed Ti_3C_2 MXene film as a TCE (Figure 4d). They had high current density and luminance characteristics at a given applied bias (Figure 4d; Figure S9, Supporting information). The maximum current efficiency was 102.0 cd A^{-1}, maximum power efficiency was 103.7 lm W^{-1}, and maximum external quantum efficiency (EQE) was 28.5%; these are comparable to those of conventional rigid ITO-based devices (103.0 cd A^{-1}, 96.9 lm W^{-1} and 29.1%) (Figure 4e,f). Our results are very close to the maximum EQE values calculated using optical simulation (29.3% for MXene-based devices; 30.2% for ITO-based devices) (Figure 4g,h). Therefore, MXene provides efficient hole-carrier injection into the EML of LEDs, and thereby yields an excellent internal charge balance in the LEDs. Also, bright, green-emitting, flexible LEDs with flexible PET/MXene anodes have been demonstrated (Figure 4i). The LED fabricated with MXene anode also showed excellent mechanical flexibility against cyclic mechanical bending and folding (Figures S10 and S11, Supporting information); this success highlights the feasibility of using MXene anodes in flexible optoelectronics.

In conclusion, we have demonstrated the feasibility of single-layered Ti_3C_2 MXene as a solution-processed flexible TCE for LEDs, and achieved high-efficiency organic LEDs based on a MXene anode for the first time by using precise surface and interface engineering. The MXene electrode produced using

a simple spin-coating and low-temperature post annealing process had highly desirable electrode properties of high WF (≈5.1 eV) and high σ (up to 11 668 S cm^{-1}), as well as good T (up to 85%). Organic LEDs with the surface-modulated MXene anode and neutralized polymeric HIL achieved high current efficiency (≈102.0 cd A^{-1}), power efficiency (103.7 lm W^{-1}) and EQE (28.5% ph/el), which approach the theoretical maxima in this device structure. The outstanding results of the MXene film and the MXene anode-based flexible organic LEDs demonstrate the strong potential of the solution-processed MXene TCE for use in next-generation optoelectronics that are produced using a low-cost solution-processing technology.

Experimental Section

Ti_3C_2 Synthesis: First, 2 g of Ti_3AlC_2 MAX phase (<38 µm) was slowly added over the course of 10 min to 40 mL of etchant solution (24 mL hydrochloric acid (HCl, 37 wt% Fisher Scientific), 12 mL deionized H_2O, 4 mL hydrofluoric acid (HF, 48–51 wt% Sigma Aldrich)). The reaction was stirred at 35 °C for 24 h using a Teflon magnetic stir bar. After the selective etching reaction, the sediment was washed by repeated centrifugation (5 min, 3500 rpm, 150 mL deionized H_2O), the acidic supernatant was decanted, and the process was repeated until the pH reached neutral (≈6). Then 2 g of lithium chloride (LiCl, Sigma Aldrich) was dissolved in 100 mL of deionized H_2O and added to the multilayer MXene sediment. The solution was stirred for 12 h at ambient temperature. The solution was washed with repeated centrifugation (5 min, 3500 rpm, 150 mL deionized H_2O) and the supernatant was decanted until a dark supernatant was observed. Then the solution was centrifuged for 1 h at 3500 rpm and the dilute green supernatant was decanted. The swollen sediment was re-dispersed with 150 mL of deionized H_2O and centrifuged for 10 min at 3500 rpm to isolate the MXene supernatant from the sediment. To optimize the flake size, the MXene supernatant was centrifuged for 30 min at 3500 rpm. The final supernatant was used in fabrication of TCEs.

Ti_3C_2 Film Preparation: Glass substrates were immersed sequentially in acetone and isopropyl alcohol (IPA) baths and sonicated for 10 min, each. The substrates were surface-treated by ultraviolet ozone for 10 min. Then 250 µL of the Ti_3C_2 solution (14 mg mL^{-1}) was deposited on the substrate and allowed to equilibrate for 30 s, then it was dispersed by spin-coating at 6000 rpm for 30 s, then at 7000 rpm for 5 s to yield in a thin, conductive electrode film. All films were dried at room temperature or vacuum-annealed 100 °C for 1 h or 200 °C for 2 h. The films were stored in a nitrogen glovebox at room temperature.

Characterizations: The surface topographic images of MXene films were obtained by atomic force microscopy (NanoScope, Digital Instruments) and field-emission scanning electron microscopy (MERLIN compact, ZEISS) at the Research Institute of Advanced Materials, Seoul National University. The optical transmittances of MXene films were measured using an ultraviolet (UV) absorption spectroscopy (Lambda 465, PerkinElmer, Inc.) and the sheet resistances of the films were obtained by four-point probe measurement combined with a Keithley 2400 source meter. The thickness was calculated using Beer–Lambert law calibration curve[32] (Ti_3C_2 absorbs 3% of visible light (at 550 nm) per nanometer thickness;, i.e., has an absorption coefficient of 1.1 × 10^{-5} cm^{-1}). Surface potentials were obtained using a Kelvin probe and air photoemission system (APS) (KP Technology Ltd.). For surface composition analysis, X-ray photoelectron spectroscopy (XPS) spectra were analyzed using a micro-X-ray/UV photoelectron spectroscopy system at the Korea Basic Science Institute.

Device Fabrications: Conducting polymer hole-injection layers (neutralized-gradient WF hole-injection layer (n-GraHIL) or poly(3,4-ethylenedioxythiophene) polystyrene sulfonate (PEDOT:PSS)) were spin-coated on patterned Ti_3C_2 substrates to give 100 nm-thick film. To fabricate organic LEDs, the substrate/anode/HIL samples were transferred to a thermal evaporator for deposition of organic layers and metal electrodes. The organic layers of TAPC (15 nm)/TCTA:Ir(ppy)$_2$acac (5 nm, 97:3 by volume)/CBP:Ir(ppy)$_2$acac (5 nm, 96:4, by volume)/TPBi (55 nm) (TAPC = 4,4′-cyclohexylidenebis(*N*,*N*-bis(4-methylphenyl) benzenamine), TCTA = tris(4-carbazoyl-9-ylphenyl)amine, CBP = 4, 4′-bis(*N*-carbazolyl)-1,1′-biphenyl, TPBi = 2,2,2-(1,3,5-benzenetriyl)tris-(1-phenyl-1H-benzimidazole)) were deposited using a thermal evaporator under 5.0 × 10^{-7} Torr. Metal electrodes of lithium fluoride, LiF (1 nm)/aluminum (100 nm) were deposited sequentially.

Optical Simulation: Optical simulation was performed using the classical dipole model that is known to predict the emission characteristic of OLEDs quantitatively.[59,60] In this optical simulation, both Purcell factor and the orientation of an emitting dipole were properly taken into account, as described in other literatures.[61,62] Both consecutive emitting TCTA and CBP layers were assumed as a single TCTA layer having the same total thickness of 10 nm, for simplicity. Then, the emission from the whole emitting layer was assumed to occur at the center of the equivalent single emitting layer. Also, it was assumed that there is no electrical loss and all generated excitons can contribute to radiative recombination. The radiative quantum yield of 0.94 and horizontal dipole ratio of 0.76 were used respectively for an emitter Ir(ppy)$_2$acac, following the previous work by Kim et al.[63]

Supporting Information

Supporting Information is available from the Wiley Online Library or from the author.

Acknowledgements

S.A., T.-H.H., and K.M. contributed equally to this work. This work was supported by the National Research Foundation of Korea (NRF) grant funded by Ministry of Science and ICT (NRF-2016R1A3B1908431). MXene synthesis work at Drexel University was supported by the Leading Foreign Research Institute Recruitment Program through the National Research Foundation of Korea funded by Ministry of Science and ICT (NNFC-Drexel-SMU FIRST Nano Coop Center, 2015K1A4A3047100).

Conflict of Interest

The authors declare no conflict of interest.

Keywords

flexible electrodes, flexible light-emitting diodes, MXene, surface engineering, titanium carbide

Received: February 9, 2020
Revised: March 12, 2020
Published online: April 30, 2020

[1] A. R. Schlatmann, D. W. Floet, A. Hilberer, F. Garten, P. J. M. Smulders, T. M. Klapwijk, G. Hadziioannou, *Appl. Phys. Lett.* **1996**, *69*, 1764.
[2] T.-H. Han, M.-R. Choi, S.-H. Woo, S.-Y. Min, C.-L. Lee, T.-W. Lee, *Adv. Mater.* **2012**, *24*, 1487.
[3] Z. Chen, *Thin Solid Films* **2001**, *394*, 202.
[4] F. Z. Dahou, L. Cattin, J. Garnier, J. Ouerfelli, M. Morsli, G. Louarn, A. Bouteville, A. Khellil, J. C. Bernède, *Thin Solid Films* **2010**, *518*, 6117.
[5] Y. Meng, Z. Hu, N. Ai, Z. Jiang, J. Wang, J. Peng, Y. Cao, *ACS Appl. Mater. Interfaces* **2014**, *6*, 5122.

[6] T.-H. Han, Y. Lee, M.-R. Choi, S.-H. Woo, S.-H. Bae, B. H. Hong, J.-H. Ahn, T.-W. Lee, *Nat. Photonics* **2012**, *6*, 105.
[7] S. Kim, S. Y. Kim, M. H. Chung, J. Kim, J. H. Kim, *J. Mater. Chem. C* **2015**, *3*, 5859.
[8] Y. Wang, C. Zhu, R. Pfattner, H. Yan, L. Jin, S. Chen, F. Molina-Lopez, F. Lissel, J. Liu, N. I. Rabiah, Z. Chen, J. W. Chung, C. Linder, M. F. Toney, B. Murmann, Z. Bao, *Sci. Adv.* **2017**, *3*, e1602076.
[9] X. Y. Chin, A. Perumal, A. Bruno, N. Yantara, S. Veldhuis, L. Martinez-Sarti, B. Chandran, V. S. Chirvony, S.-Z. A. Lo, J. So, C. Soci, M. Grätzel, H. J. Bolink, N. Mathews, S. G. Mhaisalkar, *Energy Environ. Sci.* **2018**, *11*, 1770.
[10] I. J. Kramer, D. Zhitomirsky, J. D. Bass, P. M. Rice, T. Topuria, L. Krupp, S. M. Thon, A. H. Ip, R. Debnath, H.-C. Kim, orgent, *Adv. Mater.* **2012**, *24*, 2315.
[11] G. L. Frey, K. J. Reynolds, R. H. Friend, *Adv. Mater.* **2002**, *14*, 265.
[12] F. S. F. Morgenstern, D. Kabra, S. Massip, T. J. K. Brenner, P. E. Lyons, J. N. Coleman, R. H. Friend, *Appl. Phys. Lett.* **2011**, *99*, 183307.
[13] H.-K. Seo, H. Kim, J. Lee, M.-H. Park, S.-H. Jeong, Y.-H. Kim, S.-J. Kwon, T.-H. Han, S. Yoo, T.-W. Lee, *Adv. Mater.* **2017**, *29*, 1605587.
[14] C. K. Cho, W. J. Hwang, K. Eun, S. H. Choa, S. I. Na, H. K. Kim, *Sol. Energy Mater. Sol. Cells* **2011**, *95*, 3269.
[15] S.-H. Jeong, S.-H. Woo, T.-H. Han, M.-H. Park, H. Cho, Y.-H. Kim, H. Cho, H. Kim, S. Yoo, T.-W. Lee, *NPG Asia Mater.* **2017**, *9*, e411.
[16] V. Singh, S. Arora, M. Arora, V. Sharma, R. P. Tandon, *Semicond. Sci. Technol.* **2014**, *29*, 045020.
[17] T.-H. Han, M.-H. Park, S.-J. Kwon, S.-H. Bae, H.-K. Seo, H. Cho, J.-H. Ahn, T.-W. Lee, *NPG Asia Mater.* **2016**, *8*, e303.
[18] Z. Sun, Z. Yan, J. Yao, E. Beitler, Y. Zhu, J. M. Tour, *Nature* **2010**, *468*, 549.
[19] Y. Zhu, D. K. James, J. M. Tour, *Adv. Mater.* **2012**, *24*, 4924.
[20] N. Liu, A. Chortos, T. Lei, L. Jin, T. R. Kim, W.-G. Bae, C. Zhu, S. Wang, R. Pfattner, X. Chen, R. Sinclair, Z. Bao, *Sci. Adv.* **2017**, *3*, e1700159.
[21] B. Hu, H. Ago, Y. Ito, K. Kawahara, M. Tsuji, E. Magome, K. Sumitani, N. Mizuta, K. Ikeda, S. Mizuno, *Carbon* **2012**, *50*, 57.
[22] T.-H. Han, H. Kim, S.-J. Kwon, T.-W. Lee, *Mater. Sci. Eng., R* **2017**, *118*, 1.
[23] S.-J. Kwon, T.-H. Han, T. Y. Ko, N. Li, Y. Kim, D. J. Kim, S.-H. Bae, Y. Yang, B. H. Hong, K. S. Kim, S. Ryu, T.-W. Lee, *Nat. Commun.* **2018**, *9*, 2037.
[24] P.-H. Ho, Y.-C. Yeh, D.-Y. Wang, S.-S. Li, H.-A. Chen, Y.-H. Chung, C.-C. Lin, W.-H. Wang, C.-W. Chen, *ACS Nano* **2012**, *6*, 6215.
[25] K. K. Kim, A. Reina, Y. Shi, H. Park, L.-J. Li, Y. H. Lee, J. Kong, *Nanotechnology* **2010**, *21*, 285205.
[26] T.-H. Han, S.-J. Kwon, N. Li, H.-K. Seo, W. Xu, K. S. Kim, T.-W. Lee, *Angew. Chemie Int. Ed.* **2016**, *55*, 6197.
[27] D. Alemu, H.-Y. Wei, K.-C. Ho, C.-W. Chu, *Energy Environ. Sci.* **2012**, *5*, 9662.
[28] J. McCarthy, C. Hanley, L. Brennan, V. Lambertini, Y. Gun'ko, *J. Mater. Chem. C* **2014**, *2*, 764.
[29] J. Rivnay, S. Inal, B. A. Collins, M. Sessolo, E. Stavrinidou, X. Strakosas, C. Tassone, D. M. Delongchamp, G. G. Malliaras, *Nat. Commun.* **2016**, *7*, 11287.
[30] M. Naguib, M. Kurtoglu, V. Presser, J. Lu, J. Niu, M. Heon, L. Hultman, Y. Gogotsi, M. W. Barsoum, *Adv. Mater.* **2011**, *23*, 4248.
[31] B. Anasori, Y. Gogotsi, *2D Metal Carbides and Nitrides (MXenes)*, Springer, Cham, Switzerland **2019**.
[32] A. D. Dillon, M. J. Ghidiu, A. L. Krick, J. Griggs, S. J. May, Y. Gogotsi, M. W. Barsoum, A. T. Fafarman, *Adv. Funct. Mater.* **2016**, *26*, 4162.
[33] K. Hantanasirisakul, M. Q. Zhao, P. Urbankowski, J. Halim, B. Anasori, S. Kota, C. E. Ren, M. W. Barsoum, Y. Gogotsi, *Adv. Electron. Mater.* **2016**, *2*, 1600050.
[34] A. Lipatov, M. Alhabeb, M. R. Lukatskaya, A. Boson, Y. Gogotsi, A. Sinitskii, *Adv. Electron. Mater.* **2016**, *2*, 1600255.
[35] K. Maleski, V. N. Mochalin, Y. Gogotsi, *Chem. Mater.* **2017**, *29*, 1632.
[36] D. Kim, T. Y. Ko, H. Kim, G. H. Lee, S. Cho, C. M. Koo, *ACS Nano* **2019**, *13*, 13818.
[37] D. Er, J. Li, M. Naguib, Y. Gogotsi, V. B. Shenoy, *ACS Appl. Mater. Interfaces* **2014**, *6*, 11173.
[38] X. Liang, A. Garsuch, L. F. Nazar, *Angew. Chemie, Int. Ed.* **2015**, *54*, 3907.
[39] Y. Deng, T. Shang, Z. Wu, Y. Tao, C. Luo, J. Liang, D. Han, R. Lyu, C. Qi, W. Lv, F. Kang, Q.-H. Yang, *Adv. Mater.* **2019**, *31*, 1902432.
[40] D. B. Velusamy, J. K. El-Demellawi, A. M. El-Zohry, A. Giugni, S. Lopatin, M. N. Hedhili, A. E. Mansour, E. Di Fabrizio, O. F. Mohammed, H. N. Alshareef, *Adv. Mater.* **2019**, *31*, 1807658.
[41] V. Ramalingam, P. Varadhan, H.-C. Fu, H. Kim, D. Zhang, S. Chen, L. Song, D. Ma, Y. Wang, H. N. Alshareef, J.-H. He, *Adv. Mater.* **2019**, *31*, 1903841.
[42] X. Tang, D. Zhou, P. Li, X. Guo, B. Sun, H. Liu, K. Yan, Y. Gogotsi, G. Wang, *Adv. Mater.* **2020**, *32*, 1906739.
[43] Y. Cao, X. Zhu, H. Chen, X. Zhang, J. Zhou, Z. Hu, J. Pang, *Sol. Energy Mater. Sol. Cells* **2019**, *200*, 109945.
[44] S. Yang, P. Zhang, A. S. Nia, X. Feng, *Adv. Mater.* **2020**, *32*, 1907857.
[45] T. Yun, H. Kim, A. Iqbal, Y. S. Cho, G. S. Lee, M.-K. Kim, S. J. Kim, D. Kim, Y. Gogotsi, S. O. Kim, C. M. Koo, *Adv. Mater.* **2020**, *32*, 1906769.
[46] Y. Cao, X. Zhu, J. Jiang, C. Liu, J. Zhou, J. Ni, J. Zhang, J. Pang, *Sol. Energy Mater. Sol. Cells* **2020**, *206*, 110279.
[47] C. J. Zhang, B. Anasori, A. Seral-Ascaso, S. H. Park, N. McEvoy, A. Shmeliov, G. S. Duesberg, J. N. Coleman, Y. Gogotsi, V. Nicolosi, *Adv. Mater.* **2017**, *29*, 1702678.
[48] J. L. Hart, K. Hantanasirisakul, A. C. Lang, B. Anasori, D. Pinto, Y. Pivak, J. T. van Omme, S. J. May, Y. Gogotsi, M. L. Taheri, *Nat. Commun.* **2019**, *10*, 522.
[49] N. Driscoll, A. G. Richardson, K. Maleski, B. Anasori, O. Adewole, P. Lelyukh, L. Escobedo, D. K. Cullen, T. H. Lucas, Y. Gogotsi, F. Vitale, *ACS Nano* **2018**, *12*, 10419.
[50] Z. Yu, Y. Xia, D. Du, J. Ouyang, *ACS Appl. Mater. Interfaces* **2016**, *8*, 11629.
[51] A. G. Ricciardulli, S. Yang, G.-J. A. H. Wetzelaer, X. Feng, P. W. M. Blom, *Adv. Funct. Mater.* **2018**, *28*, 1706010.
[52] Z. Liu, K. Parvez, R. Li, R. Dong, X. Feng, K. Müllen, *Adv. Mater.* **2015**, *27*, 669.
[53] T. Schultz, N. C. Frey, K. Hantanasirisakul, S. Park, S. J. May, V. B. Shenoy, Y. Gogotsi, N. Koch, *Chem. Mater.* **2019**, *31*, 6590.
[54] Z. Yu, W. Feng, W. Lu, B. Li, H. Yao, K. Zeng, J. Ouyang, *J. Mater. Chem. A* **2019**, *7*, 11160.
[55] T.-W. Lee, Y. Chung, O. Kwon, J.-J. Park, *Adv. Funct. Mater.* **2007**, *17*, 390.
[56] R. Lotfi, M. Naguib, D. E. Yilmaz, J. Nanda, A. C. T. van Duin, *J. Mater. Chem. A* **2018**, *6*, 12733.
[57] S. Chertopalov, V. N. Mochalin, *ACS Nano* **2018**, *12*, 6109.
[58] S. H. Jeong, H. Kim, M. H. Park, Y. Lee, N. Li, H. K. Seo, T. H. Han, S. Ahn, J. M. Heo, K. S. Kim, T. W. Lee, *Nano Energy* **2019**, *60*, 324.
[59] J. Lee, T.-H. Han, M.-H. Park, D. Y. Jung, J. Seo, H.-K. Seo, H. Cho, E. Kim, J. Chung, S.-Y. Choi, T.-S. Kim, T.-W. Lee, S. Yoo, *Nat. Commun.* **2016**, *7*, 11791.
[60] M. Furno, R. Meerheim, S. Hofmann, B. Lüssem, K. Leo, *Phys. Rev. B* **2012**, *85*, 115205.
[61] K. A. Neyts, *J. Opt. Soc. Am. A* **1998**, *15*, 962.
[62] C.-K. Moon, S.-Y. Kim, J.-H. Lee, J.-J. Kim, *Opt. Express* **2015**, *23*, A279.
[63] K.-H. Kim, C.-K. Moon, J.-H. Lee, S.-Y. Kim, J.-J. Kim, *Adv. Mater.* **2014**, *26*, 3844.